Journal of Materials Science: Materials in Electronics (2020) 31:7731–7741
https://doi.org/10.1007/s10854-020-03309-7

Effect of Lu doping on the structure, electrical properties and energy storage performance of $AgNbO_3$ antiferroelectric ceramics

Shuaifei Mao[1] · Nengneng Luo[1,2] · Kai Han[1] · Qin Feng[1] · Xiyong Chen[1] · Biaolin Peng[2] · Laijun Liu[3] · Changzheng Hu[3] · Huanfu Zhou[3] · Fujita Toyohisa[1] · Yuezhou Wei[1]

Received: 25 February 2020 / Accepted: 24 March 2020 / Published online: 3 April 2020

Abstract
Recently, $AgNbO_3$ antiferroelectric ceramics have attracted great attention by virtue of their characters of high energy storage density and environmental friendliness. To further optimize the electrical properties, in this work, Lu_2O_3 modified $AgNbO_3$ ceramics were prepared via conventional solid state method. Crystal structure and element analysis indicated the Lu^{3+} ion preferred to enter the A-site when Lu_2O_3 content was lower than 2 mol%, otherwise, it was more likely to form $LuNbO_4$ or Lu_3NbO_7-based solid solutions. Remarkably improved stability of antiferroelectric phase was observed once Lu^{3+} ions enter into the A-site, on account of the decrease of cell volume and tolerance factor. As a consequence, an enhanced recoverable energy storage density (W_{rec}) of 3.5 J/cm^3 was achieved in 1 mol% Lu_2O_3 modified $AgNbO_3$ ceramics at 210 kV/cm, which is superior to the other lead-free ceramics under moderate electric field (< 220 kV/cm). It is believed our study will provide a good reference for the development of $AgNbO_3$-based dielectric capacitors.

1 Introduction

With the rapid development of electronic industry, much attention has been concentrated on discovering novel energy storage materials to meet the sustainable development [1–4]. As an important branch of energy storage systems, dielectric capacitors are widely used in various kinds of high power equipment because of their fast charge/discharge rate and high power density [5–8]. However, the dielectric capacitors are greatly limited in practical application due to their low energy storage density (W_{rec}) [9–12]. Among all dielectrics, antiferroelectric (AFE) energy storage ceramics with the character of high maximum polarization (P_m) and low remnant polarization (P_r) have received significant attention. At present, lead-based antiferroelectric materials have been widely investigated because of their excellent energy storage performance [13–16]. However, with the improved social awareness of environmental protection, the lead-based materials will be gradually restricted in law. Novel lead-free dielectric capacitors with high energy storage density are urgently demanded.

As a member of perovskite family, $AgNbO_3$ (AN) lead-free antiferroelectric ceramics have recently received considerable interest. The energy storage density of pure AN ceramic ranged from 1.5–2.0 J/cm^3 depending on the applied electric field [6, 17, 18]. More importantly, this material system exhibited highly adjustable characters in energy storage performance through composition modification. Recently, aliovalent A-site cation substitution is widely used to tailoring the energy storage property of $AgNbO_3$-based ceramics [19]. For examples, high energy storage densities were achieved to 2.3, 2.6 and 2.9 J/cm^3 in Ca^{2+}, Bi^{3+} and Sr^{2+} modified $AgNbO_3$ ceramics, respectively [20–22]. Of particular importance, the lanthanide metal oxides modified $AgNbO_3$ exhibited more attractive energy storage density. A high energy storage density of 4.5 J/cm^3 was achieved in $Ag_{0.88}Gd_{0.04}NbO_3$ ceramics [23]. Our previous

✉ Nengneng Luo
luonn1234@163.com

✉ Yuezhou Wei
yzwei@gxu.edu.cn

[1] Guangxi Key Laboratory of Processing for Non-Ferrous Metals and Featured Materials, Key Laboratory of New Processing Technology for Non-Ferrous Metals and Materials, Ministry of Education, School of Resources, Environment and Materials, Guangxi University, Nanning 530004, China

[2] Center on Nanoenergy Research, School of Resources, Environment and Materials, Guangxi University, Nanning 530004, China

[3] College of Materials Science and Engineering, Guilin University of Technology, Guilin 541004, China

investigations showed that high energy storage densities of 3.12 J/cm^3 and 5.2 J/cm^3 were realized in $Ag_{0.94}La_{0.02}NbO_3$ and $Ag_{0.91}Sm_{0.03}NbO_3$ ceramics, respectively [12, 19]. The inner mechanism of above-mentioned enhanced energy storage density through chemical modification is ascribed to the improved stability of antiferroelectric phase, as a consequence of reduced tolerance factor *t*. Generally, the stability of an antiferroelectric phase for perovskite structure can be evaluated by the following formula:

$$t = \frac{R_A + R_O}{\sqrt{2}(R_B + R_O)}, \quad (1)$$

where R_O, R_A and R_B, respectively, represent the average ionic radii of oxygen anion, A-site and B-site cations [12, 24, 25]. It's generally believed that a low tolerance factor is beneficial to obtaining a highly stabilized antiferroelectric phase. The mechanism of this empirical equation is considered to lie on the decrease of cell volume and cation displacement [26], which weakens ferroelectricity and improves the antiferroelectricity.

As a last element in the lanthanide, the ion radius of Lu^{3+} ($R = 0.92$ Å) is smaller than those of most lanthanides with a coordination number of 12 [27, 28]. Once it enters into A-site to replace Ag^+, the tolerance factor and cell volume will be remarkably reduced, which will, in turn, improve the stability of antiferroelectric phase. Furthermore, among the lanthanide oxides, Lu_2O_3 was reported to possess better insulating property, higher dielectric constant and lower leakage current than those of other lanthanide oxides [29–32]. Therefore, the addition of Lu_2O_3 into $AgNbO_3$ may also enhance the breakdown field strength (E_b), which is beneficial to improving the energy storage density.

According to the aforementioned consideration, Lu_2O_3 was added into $AgNbO_3$ in this work, with the aim to improve the stability of antiferroelectric phase and enhance the energy storage density. As expected, an enhanced energy storage density (W_{rec}) of 3.5 J/cm^3 was achieved in 1 mol% Lu_2O_3 modified $AgNbO_3$ ceramics. The crystal structure, microstructure and electrical properties of the as-prepared $AgNbO_3$-based ceramics were systematically investigated.

2 Experimental procedure

The $Lu_xAg_{1-3x}NbO_3$ (LuAN*x*) ceramic samples with $x = 0$, 0.01, 0.02, 0.03 and 0.04 (abbreviated as AN, LuAN1, LuAN2, LuAN3 and LuAN4) were prepared by using a conventional solid state reaction method, details of which can be found in our earlier works [19, 26]. X-ray diffractometer (Smartlab-3KW, Rigaku Ltd, Japan) with monochromatic Cu Kα radiation was used to detect the crystal structure, after the samples were crushed into powders. The microstructure and element content of the ceramics were examined by scanning electron microscopy and energy dispersive spectrometer (SEM–EDS, Pro X, Phenom, Eindhoven, Netherlands). The dielectric-temperature spectrum was obtained by using the LCR tester (Model 4294A, Hewlett-Packard Co.) as the temperature elevate from 30 to 500 °C. Ferroelectric analyzer (RT66, Radiant Technologies, USA) was employed to obtain the polarization versus electric field hysteresis loops (*P*–*E* loops) and the current versus electric field (*I*–*E* curves) at 1 Hz.

3 Results and discussion

3.1 Crystal structure and microstructure analysis

The compositional dependence of X-ray diffraction patterns are displayed in Fig. 1. Pure perovskite structure can be observed in undoped $AgNbO_3$, as compared with JCPDS file No. 70-4738. However, once a certain amount of Lu_2O_3 is added, a few small extra peaks come across, as shown in the enlarged patterns with angles in the range of 29°–31°. When 1 mol% Lu_2O_3 is doped, an extra peak identified as $LuNbO_4$ is observed, which may be associated with a higher reaction activity between Lu_2O_3 and Nb_2O_5 raw materials compared with that between Ag_2O and Nb_2O_5. As the content of Lu increases to 2 mol%, other peaks identified as Lu_3NbO_7 are also observed. The XRD Rietveld refinement on the basis of *Pbcm* space group was obtained by using GSAS software to further study the crystal structure evolution of $AgNbO_3$ with the increase of Lu_2O_3 doping amount, which was displayed in Fig. 2a–e. The low reliability factor values indicate the structural model is valid and the refinement results fit well with the experimental data. The Rietveld lattice parameters *a*, *b*, *c* and the cell volume *V* are calculated, as exhibited

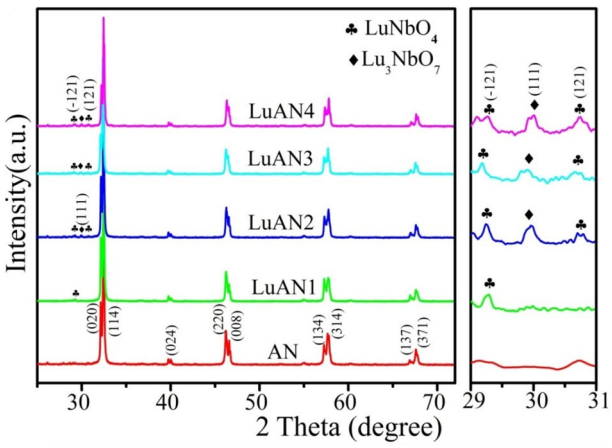

Fig. 1 Compositional dependence of X-ray diffraction patterns and enlargement of the 29°–31° range of LuAN*x* ceramics

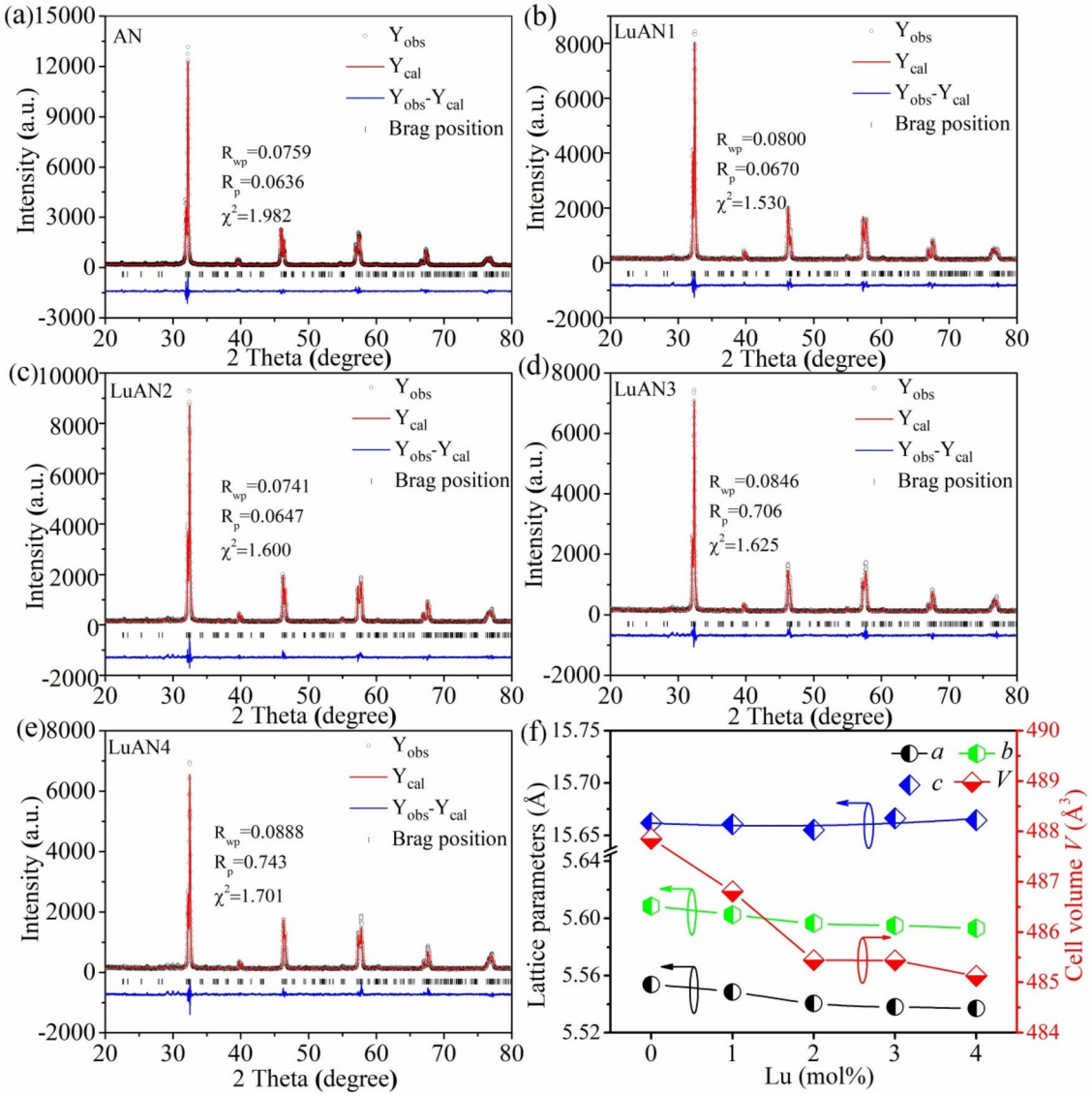

Fig. 2 XRD Rietveld refinement of **a** AN, **b** LuAN1, **c** LuAN2, **d** LuAN3, **e** LuAN4 ceramics and **f** lattice parameters *a*, *b*, *c* and unit cell volume *V* as a function of Lu_2O_3 content

in Fig. 2f. The *a* and *b* slightly decrease with the increase of Lu_2O_3 doping amount, while the *c* changes very little. More interestingly, the cell volume *V* decreases remarkably at low Lu level (< 2 mol%), which then exhibits very small change by further adding Lu_2O_3. In general, the smaller Lu^{3+} ($R = 0.92$ Å) ions prefer to substitute for Ag^+ ($R = 1.48$ Å) in the A-site, as described by the solid solution formula as follows:

$$Lu_2O_3 + 3Nb_2O_5 \rightarrow 2Lu^{\cdot\cdot}_{Ag} + 4V'_{Ag} + 6Nb^{\times}_{Nb} + 18O^{\times}_{O}. \quad (2)$$

The substitution of Ag^+ by Lu^{3+} and the produced silver vacancies contribute to the sharp decrease of cell volume *V*, which is in favor of the stability of antiferroelectric phase. However, both lattice distortion and valance imbalance will increase with the Lu^{3+} ions successive diffusing into the crystal lattice, because of the large ionic radius and valance variations between Ag^+ and Lu^{3+} ions. This will restrict extra Lu^{3+} ions from entering into $AgNbO_3$ lattice, resulting into a limited solid solubility of Lu^{3+} ions. As a consequence, the cell volume *V* stays almost no change and secondary phases come to across gradually, which is the case of $x > 2$ mol%, as confirmed by the cell volume variations and the extra peaks in XRD patterns.

Figure 3a–e display the microstructure of the as-sintered LAN*x* ceramics. Few porosities are observed on the surface morphology, which indicates a high relative bulk density.

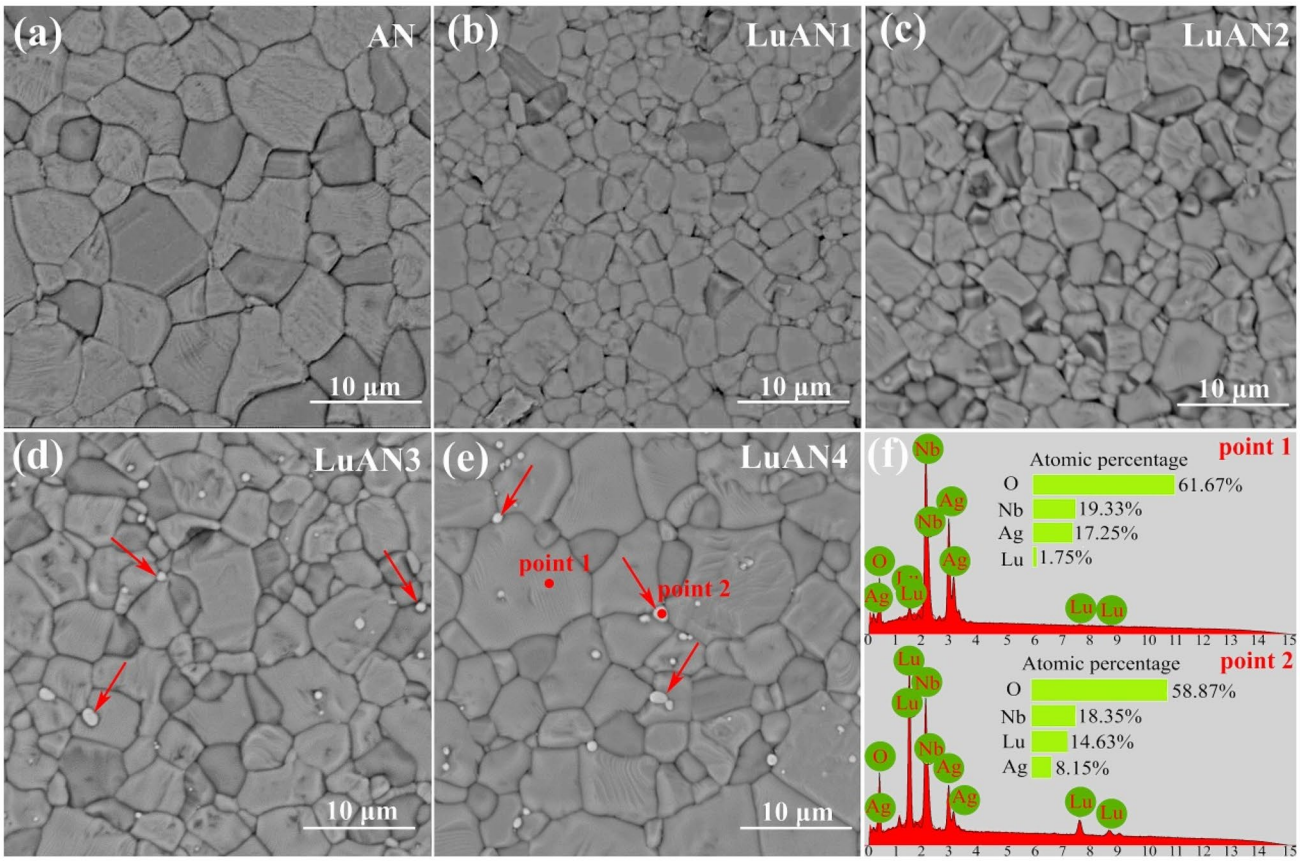

Fig. 3 SEM surface images of **a** AN, **b** LuAN1, **c** LuAN2, **d** LuAN3, **e** LuAN4 ceramics and **f** the various atomic percentage at different grains of LuAN4 ceramics (Color figure online)

Some small grains with different contrast are also observed when $x > 2$ mol%, as marked with red arrows in Fig. 3d and e for LuAN3 and LuAN4, respectively. In order to explore the difference between the abnormal grains and the matrix, the EDS is applied on various grains of LuAN4 ceramics. The obtained EDS patterns and calculated atomic percentage are shown in Fig. 3f. The atomic ratio (Ag:Nb:O) of mother grains (point 1 in Fig. 3e) is near to 1:1:3, which is consistent with the chemical formula of $AgNbO_3$. Besides, signature of Lu element with atomic percentage around 1.75% is also detected, indicating that a portion of Lu^{3+} diffuses into the $AgNbO_3$ lattice and the solid solubility of Lu^{3+} is around 2 mol%. While the atomic percentage of Lu, Nb, O and Ag elements in abnormal grain (point 2 in Fig. 3e) are, respectively, found to be 14.63%, 18.35%, 58.87% and 8.15%, which is almost identical with the chemical formula $LuNbO_4$ with a certain amount of Ag^+ entering into the lattice. However, the Lu_3NbO_7 is not confirmed yet, which may because its amount is too low to be detected by EDS.

The breakdown strength is closely related to the grain size, so it's very important to count the grain size distribution. Herein, the grain size variations of the AN-based ceramics before and after Lu_2O_3 modification are determined and shown in Fig. 4a–e. The statistical grain size generally obeys Gaussian distribution for all compositions. The relationship between average grain size and Lu_2O_3 doping amount is illustrated in Fig. 4f. The average grain size is about 6 μm for AN ceramics. The average grain size significantly reduces to ~ 2.3 μm after 1 mol% Lu_2O_3 addition, which may be resulted from the silver vacancies combined with the impurity ions (Lu^{3+} ions in the lattice) which inhibit the mass transport [33, 34]. However, the average grain size tends to increase with further increase of Lu_2O_3 content. This may be associated with the limited solid solubility of Lu^{3+} ions in the $AgNbO_3$ lattice. The excess Lu^{3+} ions prefer to precipitate from the mother grain and exist in the grain boundary during the sintering process, which may accelerate the grain boundary mobility, thus leading to the growth of mother grain. Due to the hindrance of the secondary phase, the grain size is still smaller than that of pure $AgNbO_3$.

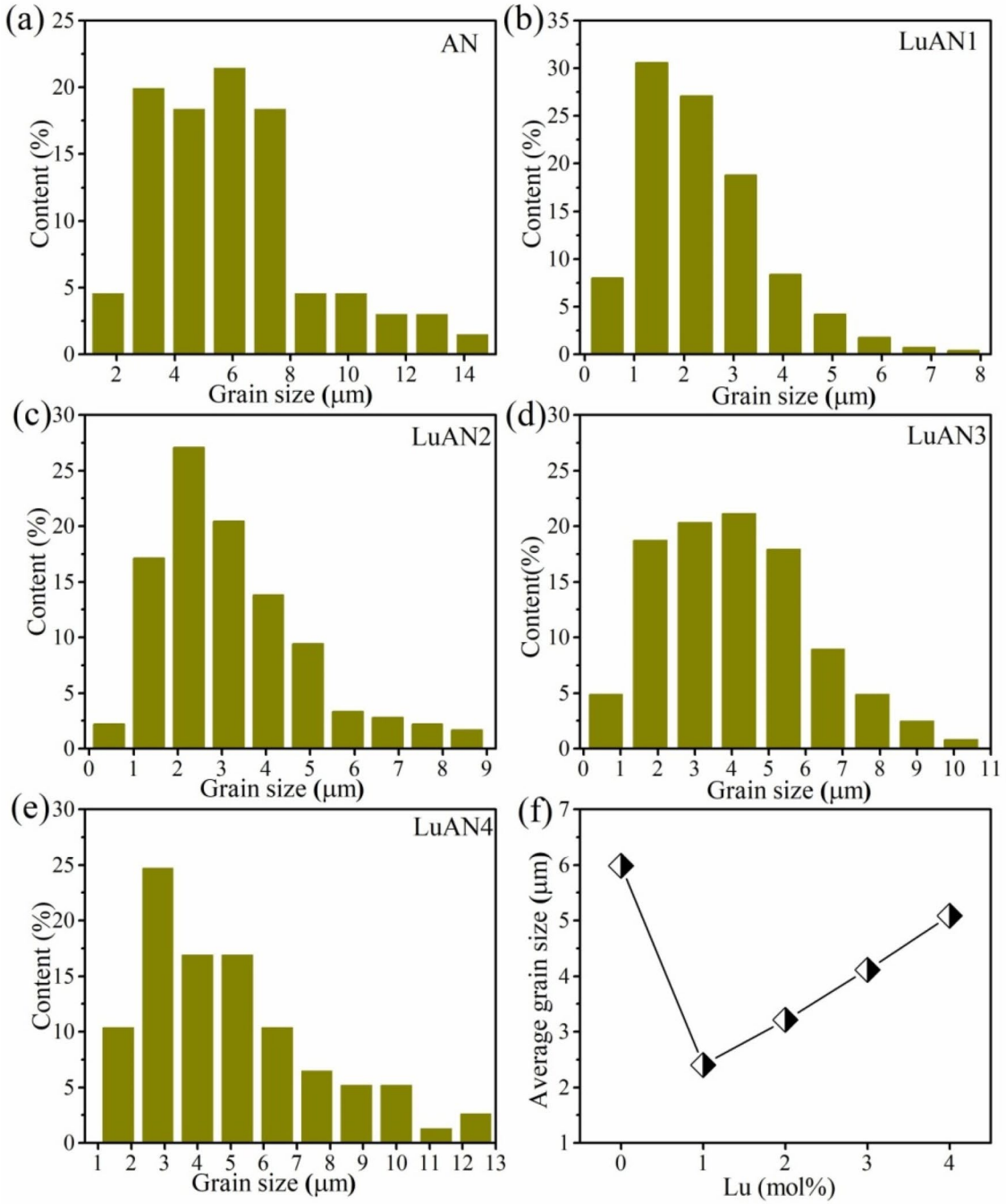

Fig. 4 Grain size distribution of **a** AN, **b** LuAN1, **c** LuAN2, **d** LuAN3, **e** LuAN4 ceramics and **f** the average grain size as a function of Lu_2O_3 content

3.2 Dielectric properties

In order to investigate dielectric properties and the stability of antiferroelectricity in the Lu_2O_3 modified $AgNbO_3$ ceramics, the dielectric permittivity and loss are measured at different frequencies from 1 kHz to 1 MHz, as shown in Fig. 5a–e. Four dielectric anomalies are observed in AN, LuAN1 and LuAN2 ceramics, which is consistent with the existing reports [3, 8, 19].

It should be noticed that an extra dielectric anomaly at temperature around 270 °C is observed when $x > 2$ mol%, which may be associated with the secondary phase. All samples exhibit very low dielectric loss, indicating high electric resistance. In order to explore the influence of

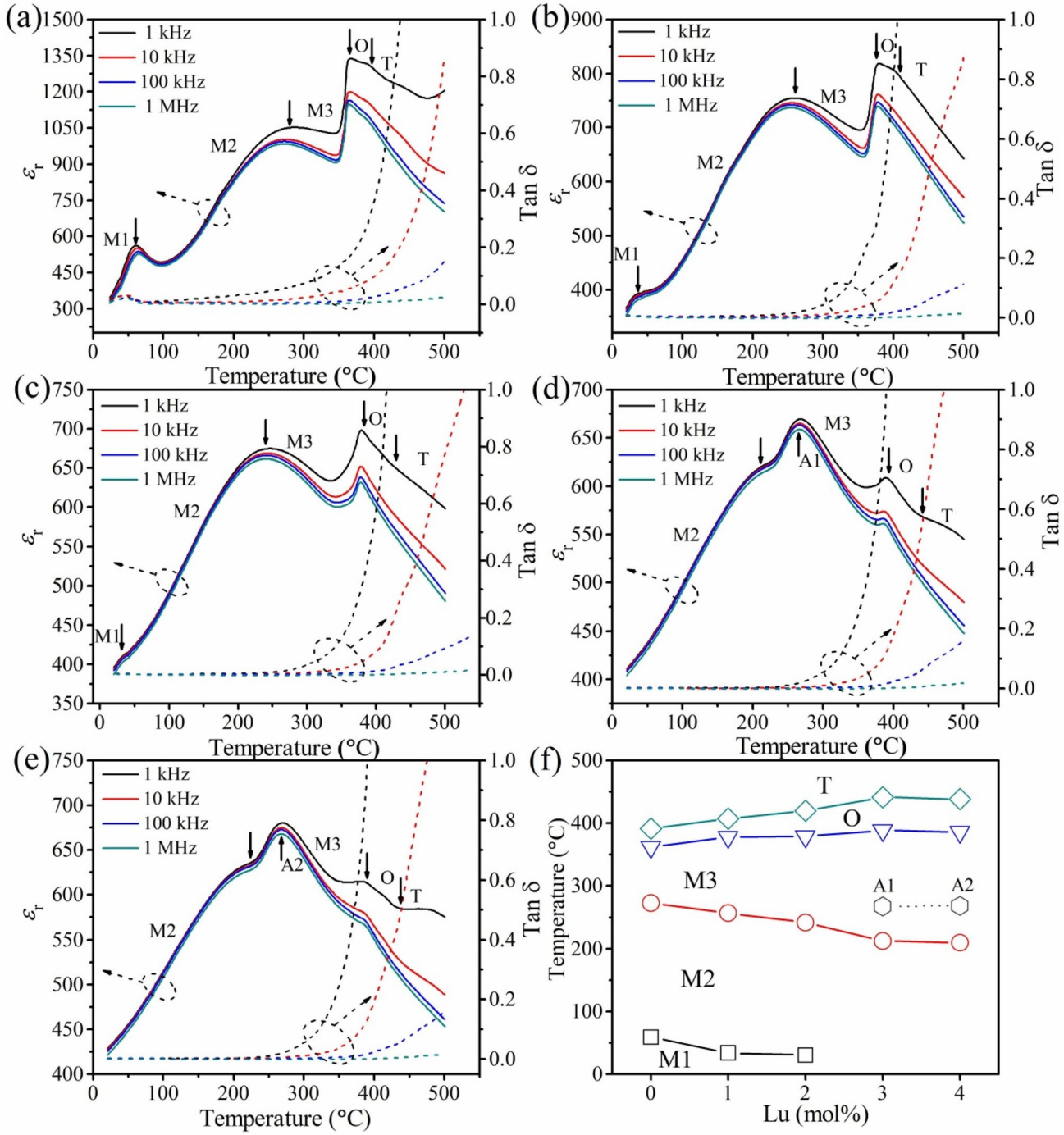

Fig. 5 Dielectric-temperature spectrum measured at different frequencies from 1 kHz to 1 MHz for **a** AN, **b** LuAN1, **c** LuAN2, **d** LuAN3, **e** LuAN4 ceramics and **f** phase diagram obtained from the dielectric-temperature spectrum

Lu_2O_3 modification on the phase transition, the phase diagram is constructed in Fig. 5f based on the dielectric-temperature spectrum. The T_{M1-M2} (M1–M2 phase transition temperature) is adjusted to below room temperature when Lu_2O_3 doping amount is over 2 mol%. The lower T_{M1-M2} indicates a much more stable antiferroelectric phase at room temperature for Lu_2O_3 doped compositions, which may benefit the improvement in energy storage density. The M2–M3 phase transition temperature (T_{M2-M3}) is also found to decrease with increase of Lu_2O_3 level. Furthermore, the M3–O phase (T_{M3-O}) and O–T (T_{O-T}) transition temperatures increase slightly with the increase of Lu_2O_3

content. The temperatures for the extra dielectric anomaly stay stable with increasing Lu_2O_3 content, which further verify it may be caused by the secondary phases; more investigations need to be done to confirm this.

3.3 Electrical properties

To investigate the ferroelectric and energy storage properties of the Lu_2O_3 modified $AgNbO_3$ ceramics, the *P*–*E* loops and *I*–*E* curves are shown in Fig. 6a–e. Typical double-like *P*–*E* loops are obtained when $x < 3$ mol%, which is consistent

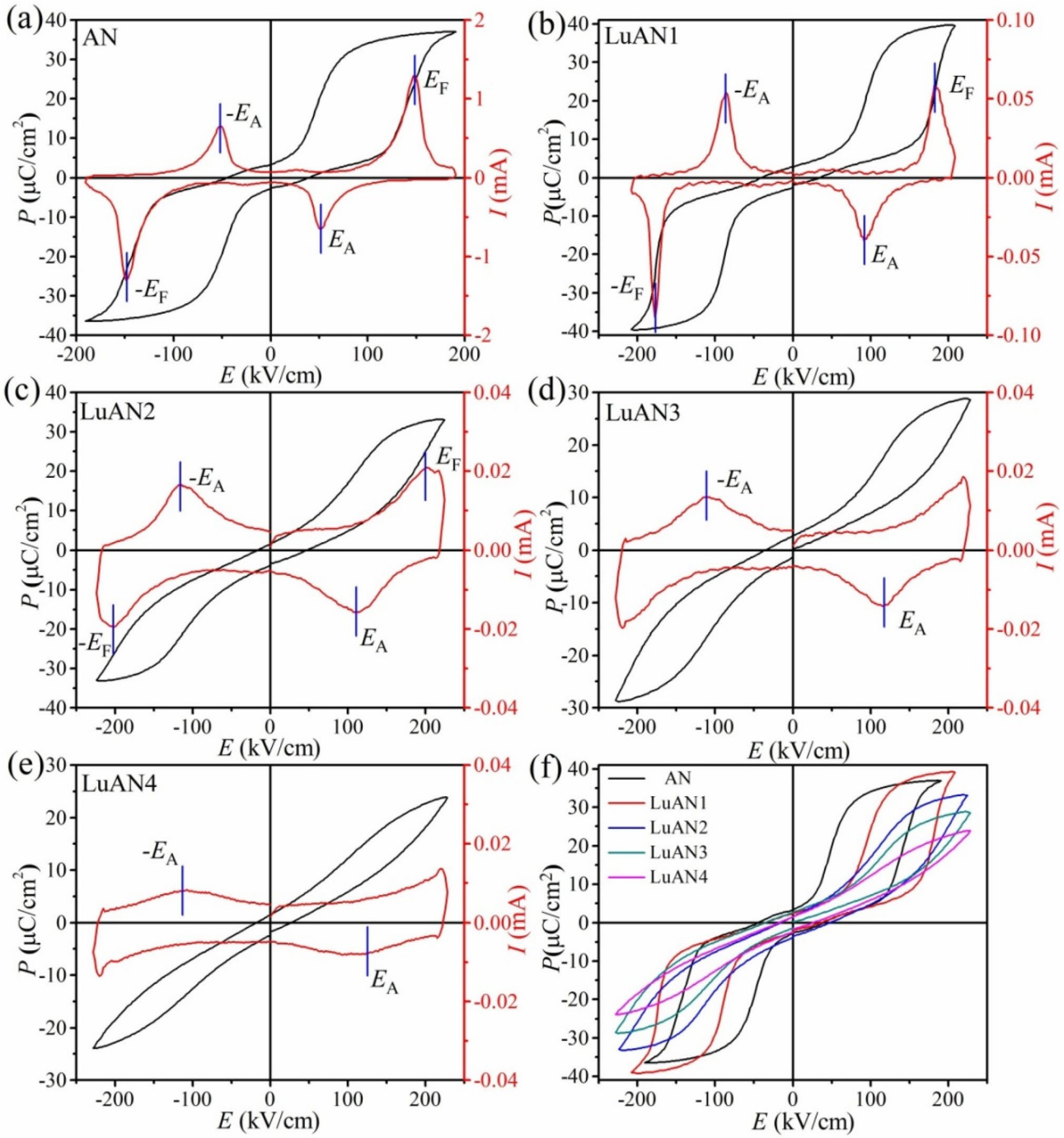

Fig. 6 *P*–*E* loops and *I*–*E* curves of **a** AN, **b** LuAN1, **c** LuAN2, **d** LuAN3, **e** LuAN4 ceramics and **f** total *P*–*E* loops of the LuAN*x* ceramics with different Lu_2O_3 content

with a antiferroelectric feature. The four peaks in *I–E* curves are further confirmed the antiferroelectric feature [35]. Figure 6f gives a comparison of the *P–E* loops for LuAN*x* system. The hysteresis becomes smaller with increase of the Lu_2O_3 doping amount, which is benefit to higher energy storage efficiency. In order to look into the effect of Lu_2O_3 modification on ferroelectric properties, the detailed evolution of the electrical parameters is also investigated, as displayed in Fig. 7a, b. The P_{max} initially increases from 37.0 μC/cm^2 for undoped $AgNbO_3$ to 39.7 μC/cm^2 for LuAN1 ceramic after 1 mol% Lu_2O_3 modification, which decreases continuously by further increasing Lu_2O_3 content. While the P_r exhibits a generally decrease with the increase of Lu_2O_3 doping amount, which is attributed to the enhanced stability of antiferroelectric phase. Furthermore, both E_F (AFE to FE phase transition electric field) and E_A (FE to AFE phase transition electric field) increase with the increase of Lu_2O_3 doping content when $x < 2$ mol%, as shown in Fig. 7b. Once the Lu_2O_3 doping level exceeds 2 mol%, the E_A is relative stable, due to the limited solid solubility for Lu^{3+} in $AgNbO_3$. The disappearance of E_F at higher Lu_2O_3 doping level may be resulted from the higher antiferroelectric–ferroelectric phase transition electric field, which exceeds the breakdown field strength of the ceramics.

It is generally believed that the stability of antiferroelectricity is closely related to the tolerance factor *t*. Herein, the theoretical value of *t* is calculated on the basis of Eq. (1) and is displayed in Fig. 7c, which decreases linearly if all Lu^{3+} ions enter into A-site. In fact, due to the limited solid solubility of Lu^{3+} in $AgNbO_3$ lattice, the possible value of *t* may be deviated to the theoretical value. As discussed previously, the solid solubility of Lu^{3+} in $AgNbO_3$ lattice is around 2 mol%, so the possible value of *t* should decrease firstly (~ 2 mol%) and then become relatively stable with further increase of Lu_2O_3 content, similar to the dotted curve given Fig. 7c. The change of *t* and unit cell volume *V* may account for the complex evolution of E_A and E_F.

Figure 7d gives the W_{rec} and efficiency η of Lu_2O_3 modified $AgNbO_3$ ceramics to evaluate the electric performance. The W_{rec} is up to 1.89 J/cm^3 at 190 kV/cm for

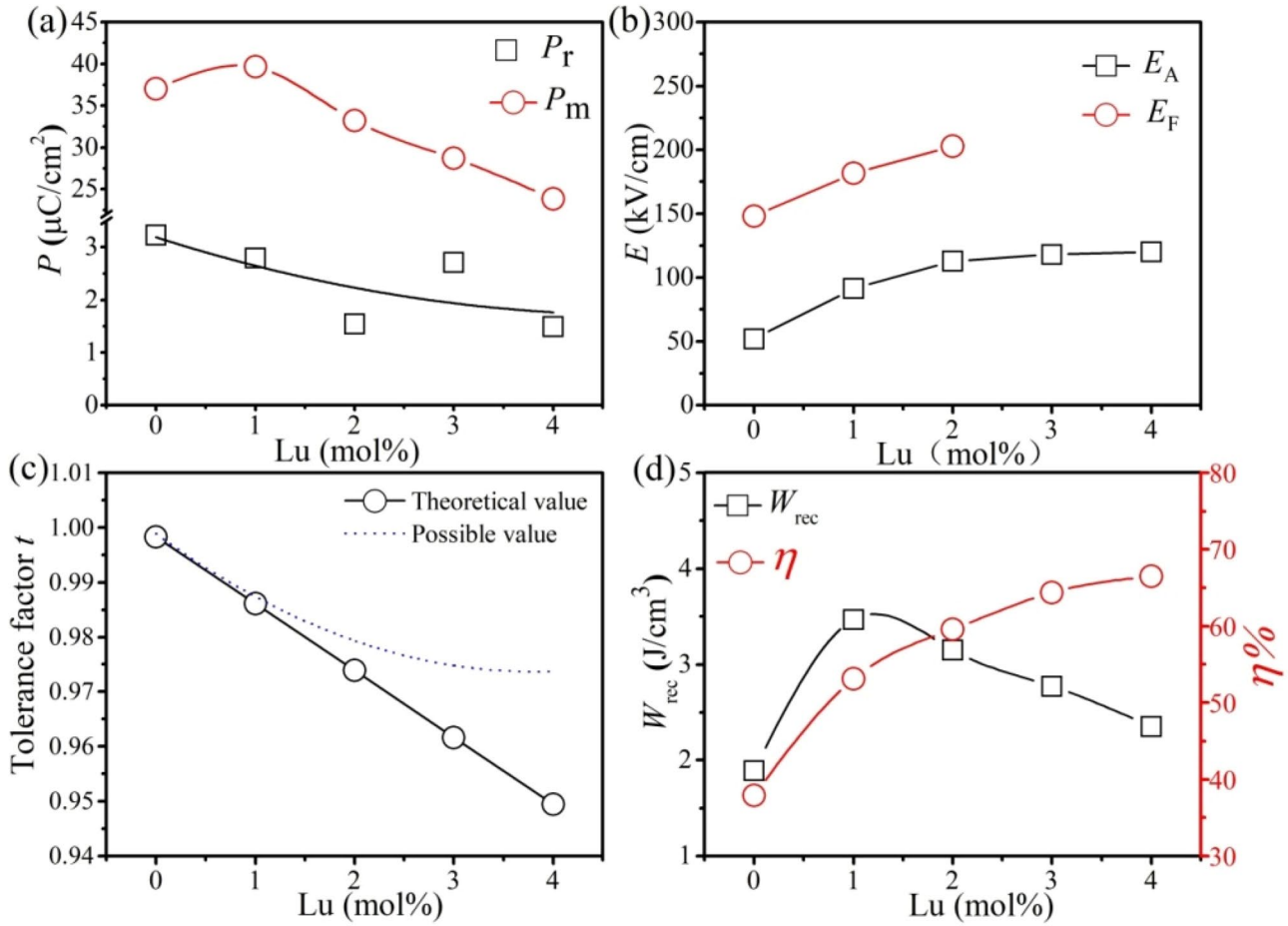

Fig. 7 **a** P_m and P_r, **b** E_A and E_F of the LuAN*x* ceramics as a function of Lu_2O_3 content, **c** the evolution of theoretical (solid) and possible (dot) value of tolerance factor *t* and **d** energy storage properties as a function of Lu_2O_3 doping amount

Table 1 Comparison of W_{rec} between LuAN*x* systems and other lead-free materials under moderate field ($E_b < 220$ kV)

Materials system	E_b (kV/cm)	W_{rec} (J/cm^3)	References
$0.90BaTiO_3$–$0.09BiInO_3$	140	0.753	[36]
$BaTiO_3$–$Bi_{0.5}Na_{0.5}TiO_3$–$Na_{0.73}Bi_{0.09}NbO_3$	172	1.7	[37]
$0.92BaTiO_3$–$0.08Bi_{0.09}K_{0.73}NbO_3$	180	2.51	[38]
$BiFeO_3$–$BaTiO_3$–Nb_2O_5	90	0.71	[39]
$BiFeO_3$–$BaTiO_3$–$Ba(Mg_{1/3}Nb_{2/3})O_3$	125	1.56	[40]
(Bi, Nd)FeO_3–$BaTiO_3$	180	1.82	[41]
$0.67Bi_{0.9}Sm_{0.1}FeO_3$–$0.33BaTiO_3$	200	2.8	[42]
$0.85Na_{0.5}Bi_{0.5}TiO_3$–$0.15BaHfO_3$	175	2.1	[43]
$0.9Na_{0.5}Bi_{0.5}TiO_3$–$0.1LiTaO_3$	200	2.3	[44]
$0.7\ K_{0.5}Na_{0.5}NbO_3$–$0.3SrTiO_3$	190	2.31	[45]
$0.94K_{0.5}Bi_{0.5}TiO_3$–$0.06La(Mg_{0.5}Ti_{0.5})O_3$	180	2.08	[46]
$0.9\ K_{0.5}Na_{0.5}NbO_3$–$0.1BiFeO_3$	206	2	[47]
$AgNbO_3$–0.1 wt% MnO_2	150	2.50	[17]
$Ag_{0.96}Ba_{0.02}NbO_3$	180	2.3	[20]
$AgNbO_3$–0.1 wt% WO_3	200	3.3	[11]
Lu_2O_3 modified $AgNbO_3$	210	3.5	This work

undoped $AgNbO_3$, which increases to 3.5 J/cm^3 accompanied with efficiency η of 53.1% after 1 mol% Lu_2O_3 addition at 210 kV/cm. With further increases of the Lu_2O_3 doping amount, the W_{rec} decreases due to the lower P_{max}. The energy storage efficiency also increases from 37.9% (AN) to 66.5% (LuAN4) because of the decreased hysteresis of *P*–*E* loops. Furthermore, a comprehensive comparison of W_{rec} among other lead-free materials system are made in Table 1 [11, 17, 20, 36–47], which indicates that Lu_2O_3 doped $AgNbO_3$ antiferroelectric ceramics are superior to the most of lead-free ceramics under moderate electric field (< 220 kV/cm).

4 Conclusion

In this work, Lu_2O_3 modified $AgNbO_3$ lead-free antiferroelectric ceramics were synthesized via solid state reaction method. A certain amount of Lu_2O_3 (< 2 mol%) led a decrease in cell volume *V* and tolerance factor *t*, while second phase came to across with higher Lu_2O_3 level due to the limited solid solubility. The Lu^{3+} ions in the lattice benefited to the improvement of stability of antiferroelectric phase, thus leading to the enhanced E_F and E_A. As a consequence, high W_{rec} up to 3.5 J/cm^3 accompanied with efficiency of 53.1% at 210 kV/cm was achieved in 1 mol% Lu_2O_3 doped $AgNbO_3$ ceramics. The results indicate that Lu_2O_3 doped $AgNbO_3$ antiferroelectric ceramics is promising for dielectric capacitors.

Acknowledgements This work was supported by National Nature Science Foundation of China (Grant 11864004), Nature Science Foundation of Guangxi (Grant 2017GXNSFBA198132), Science and Technology Major Project of Guangxi (Grant AA17204110), and Innovation Project of Guangxi Graduate Education (Grant YCSW2019053).

Compliance with ethical standards

Conflict of interest The authors declare that they have no conflicts of interest.

References

1. J. Cherusseri, N. Choudhary, K. Sambath Kumar, Y. Jung, J. Thomas, Recent trends in transition metal dichalcogenide based supercapacitor electrodes. Nanoscale Horiz. **4**, 840–858 (2019)
2. X. Jian, H. Wang, G. Rao, L. Jiang, H. Wang, C.M. Subramaniyam, A. Mahmood, W. Zhang, Y. Xiang, S.X. Dou, Z. Zhou, D. Hui, K. Kalantar-Zadeh, N. Mahmood, Self-tunable ultrathin carbon nanocups as the electrode material of sodium-ion batteries with unprecedented capacity and stability. Chem. Eng. J. **364**, 578–588 (2019)
3. B. Xu, J. Iniguez, L. Bellaiche, Designing lead-free antiferroelectrics for energy storage. Nat. Commun. **8**, 15682 (2017)
4. Y. Guo, X. Jian, L. Zhang, C. Mu, L. Yin, J. Xie, N. Mahmood, S. Dou, R. Che, L. Deng, Plasma-induced FeSiAl@Al_2O_3@SiO_2 core–shell structure for exceptional microwave absorption and anti-oxidation at high temperature. Chem. Eng. J. **384**, 123371 (2020)
5. S. Aboubakr, A. Hajjaji, M. Rguiti, K. Benkhouja, C. Courtois, A high dielectric composite for energy storage application. Int. J. Hydrog. Energy **42**, 19504–19511 (2017)
6. Y. Tian, L. Jin, H. Zhang, Z. Xu, X. Wei, E.D. Politova, S.Y. Stefanovich, N.V. Tarakina, I. Abrahams, H. Yan, High energy density in silver niobate ceramics. J. Mater. Chem. A **4**, 17279–17287 (2016)
7. M. Zhou, R. Liang, Z. Zhou, S. Yan, X. Dong, Novel sodium niobate-based lead-free ceramics as new environment-friendly energy storage materials with high energy density, high power density, and excellent stability. ACS Sustain. Chem. Eng. **6**, 12755–12765 (2018)
8. Y. Ahn, J. Seo, J.Y. Son, Ferroelectric domain switching kinetics of a lead-free $AgNbO_3$ thin film on glass substrate. Appl. Surf. Sci. **357**, 429–432 (2015)

9. M. Zhou, R. Liang, Z. Zhou, C. Xu, X. Nie, X. Chen, X. Dong, High energy storage properties of $(Ni_{1/3}Nb_{2/3})^{4+}$ complex-ion modified $(Ba_{0.85}Ca_{0.15})$ $(Zr_{0.10}Ti_{0.90})O_3$ ceramics. Mater. Res. Bull. **98**, 166–172 (2018)
10. Y. Xie, J. Wang, Y. Yu, W. Jiang, Z. Zhang, Enhancing breakdown strength and energy storage performance of PVDF-based nanocomposites by adding exfoliated boron nitride. Appl. Surf. Sci. **440**, 1150–1158 (2018)
11. L. Zhao, J. Gao, Q. Liu, S. Zhang, J.F. Li, Silver niobate lead-free antiferroelectric ceramics: enhancing energy storage density by B-site doping. ACS Appl. Mater. Interfaces **10**, 819–826 (2018)
12. N. Luo, K. Han, L. Liu, B. Peng, X. Wang, C. Hu, H. Zhou, Q. Feng, X. Chen, Y. Wei, Lead-free $Ag_{1-3x}La_xNbO_3$ antiferroelectric ceramics with high-energy storage density and efficiency. J. Am. Ceram. Soc. **102**, 4640–4647 (2019)
13. B. Peng, Q. Zhang, X. Li, T. Sun, H. Fan, S. Ke, M. Ye, Y. Wang, W. Lu, H. Niu, X. Zeng, H. Huang, Large energy storage density and high thermal stability in a highly textured (111)-oriented $Pb_{0.8}Ba_{0.2}ZrO_3$ relaxor thin film with the coexistence of antiferroelectric and ferroelectric phases. ACS Appl. Mater. Interfaces **7**, 13512–13517 (2015)
14. Y. Liu, Y. Wang, X. Hao, J. Xu, Preparation and energy-storage performance of PLZT antiferroelectric thick films via sol–gel method. Ceram. Int. **39**, S513–S516 (2013)
15. X. Hao, Y. Wang, L. Zhang, L. Zhang, S. An, Composition-dependent dielectric and energy-storage properties of (Pb, La)(Zr, Sn, Ti)O_3 antiferroelectric thick films. Appl. Phys. Lett. **102**, 163903 (2013)
16. X. Yang, C. He, Y. Liu, X. Long, Structure and properties of $(Na_xLa_xPb_{1-2x})$ $(Lu_{1/2}Nb_{1/2})O_3$ antiferroelectric ceramics. Mater. Des. **92**, 330–334 (2016)
17. L. Zhao, Q. Liu, S. Zhang, J.-F. Li, Lead-free $AgNbO_3$ anti-ferroelectric ceramics with an enhanced energy storage performance using MnO_2 modification. J. Mater. Chem. C **4**, 8380–8384 (2016)
18. Y. Tian, L. Jin, Q.Y. Hu, K. Yu, Y.Y. Zhuang, G. Viola, I. Abrahams, Z. Xu, X.Y. Wei, H.X. Yan, Phase transitions in tantalum-modified silver niobate ceramics for high power energy storage. J. Mater. Chem. A **7**, 834–842 (2019)
19. N. Luo, K. Han, F. Zhuo, C. Xu, G. Zhang, L. Liu, X. Chen, C. Hu, H. Zhou, Y. Wei, Aliovalent A-site engineered $AgNbO_3$ lead-free antiferroelectric ceramics toward superior energy storage density. J. Mater. Chem. A **7**, 14118–14128 (2019)
20. K. Han, N. Luo, Y. Jing, X. Wang, B. Peng, L. Liu, C. Hu, H. Zhou, Y. Wei, X. Chen, Q. Feng, Structure and energy storage performance of Ba-modified $AgNbO_3$ lead-free antiferroelectric ceramics. Ceram. Int. **45**, 5559–5565 (2019)
21. Y. Tian, L. Jin, H. Zhang, Z. Xu, X. Wei, G. Viola, I. Abrahams, H. Yan, Phase transitions in bismuth-modified silver niobate ceramics for high power energy storage. J. Mater. Chem. A **5**, 17525–17531 (2017)
22. K. Han, N. Luo, S. Mao, F. Zhuo, X. Chen, L. Liu, C. Hu, H. Zhou, X. Wang, Y. Wei, Realizing high low-electric-field energy storage performance in $AgNbO_3$ ceramics by introducing relaxor behaviour. J. Materiomics **5**, 597–605 (2019)
23. S. Li, H. Nie, G. Wang, C. Xu, N. Liu, M. Zhou, F. Cao, X. Dong, Significantly enhanced energy storage performance of rare-earth-modified silver niobate lead-free antiferroelectric ceramics via local chemical pressure tailoring. J. Mater. Chem. C **7**, 1551–1560 (2019)
24. H. Shimizu, H. Guo, S.E. Reyes-Lillo, Y. Mizuno, K.M. Rabe, C.A. Randall, Lead-free antiferroelectric: $xCaZrO_3$–$(1–x)NaNbO_3$ system ($0 \le x \le 0.10$). Dalton Trans. **44**, 10763–10772 (2015)
25. R. Xu, Q. Zhu, J. Tian, Y. Feng, Z. Xu, Effect of Ba-dopant on dielectric and energy storage properties of PLZST antiferroelectric ceramics. Ceram. Int. **43**, 2481–2485 (2017)
26. K. Han, N. Luo, S. Mao, F. Zhuo, L. Liu, B. Peng, X. Chen, C. Hu, H. Zhou, Y. Wei, Ultrahigh energy-storage density in A-/B-site co-doped $AgNbO_3$ lead-free antiferroelectric ceramics: insight into the origin of antiferroelectricity. J. Mater. Chem. A **7**, 26293–26301 (2019)
27. L.A. Xue, Y. Chen, R.J. Brook, The effect of lanthanide contraction on grain growth in lanthanide-doped $BaTiO_3$. J. Mater. Sci. Lett. **7**, 1163–1165 (1988)
28. L.A. Xue, Y. Chen, R.J. Brook, The influence of ionic radii on the incorporation of trivalent dopants into $BaTiO_3$. Mater. Sci. Eng. **BI**, 193–201 (1988)
29. C.L. Yuan, P. Darmawan, M.Y. Chan, P.S. Lee, Leakage conduction mechanism of amorphous Lu_2O_3 high-k dielectric films fabricated by pulsed laser ablation. Europhys. Lett. **77**, 67001 (2007)
30. P. Darmawan, P.S. Chia, P.S. Lee, Rare-earth based ultra-thin Lu_2O_3 for high-k dielectrics. J. Phys. Conf. Ser. **61**, 229–233 (2007)
31. G. Scarel, E. Bonera, C. Wiemer, G. Tallarida, S. Spiga, M. Fanciulli, I.L. Fedushkin, H. Schumann, Y. Lebedinskii, A. Zenkevich, Atomic-layer deposition of Lu_2O_3. Appl. Phys. Lett. **85**, 630–632 (2004)
32. S. Ohmi, M. Takeda, H. Ishiwara, H. Iwai, Electrical characteristics for Lu_2O_3 thin films fabricated by E-beam deposition method. J. Electrochem. Soc. **151**, G279–G283 (2004)
33. Q. Lin, M. Jiang, D. Lin, Q. Zheng, X. Wu, X. Fan, Effects of La-doping on microstructure, dielectric and piezoelectric properties of $Ba_{0.85}Ca_{0.15}Ti_{0.90}Zr_{0.10}O_3$ lead-free ceramics. J. Mater. Sci. Mater. Electron. **24**, 734–739 (2012)
34. B.W. Lee, E.J. Lee, Effects of complex doping on microstructural and electrical properties of PZT ceramics. J. Electroceram. **17**, 597–602 (2006)
35. G. Viola, T. Saunders, X. Wei, K.B. Chong, H. Luo, M.J. Reece, H. Yan, Contribution of piezoelectric effect, electrostriction and ferroelectric/ferroelastic switching to strain-electric field response of dielectrics. J. Adv. Dielectr. **03**, 1350007 (2013)
36. M. Wei, J. Zhang, K. Wu, H. Chen, C. Yang, Effect of $BiMO_3$ (M=Al, In, Y, Sm, Nd, and La) doping on the dielectric properties of $BaTiO_3$ ceramics. Ceram. Int. **43**, 9593–9599 (2017)
37. H. Yang, F. Yan, Y. Lin, T. Wang, F. Wang, Y. Wang, L. Guo, W. Tai, H. Wei, Lead-free $BaTiO_3$–$Bi_{0.5}Na_{0.5}TiO_3$–$Na_{0.73}Bi_{0.09}NbO_3$ relaxor ferroelectric ceramics for high energy storage. J. Eur. Ceram. Soc. **37**, 3303–3311 (2017)
38. Y. Lin, D. Li, M. Zhang, S. Zhan, Y. Yang, H. Yang, Q. Yuan, Excellent energy-storage properties achieved in $BaTiO_3$-based lead-free relaxor ferroelectric ceramics via domain engineering on the nanoscale. ACS Appl. Mater. Interfaces **11**, 36824–36830 (2019)
39. T. Wang, L. Jin, Y. Tian, L. Shu, Q. Hu, X. Wei, Microstructure and ferroelectric properties of Nb_2O_5-modified $BiFeO_3$–$BaTiO_3$ lead-free ceramics for energy storage. Mater. Lett. **137**, 79–81 (2014)
40. D. Zheng, R. Zuo, D. Zhang, Y. Li, X. Tan, Novel $BiFeO_3$–$BaTiO_3$–$Ba(Mg_{1/3}Nb_{2/3})O_3$ lead-free relaxor ferroelectric ceramics for energy-storage capacitors. J. Am. Ceram. Soc. **98**, 2692–2695 (2015)
41. D. Wang, Z. Fan, D. Zhou, A. Khesro, S. Murakami, A. Feteira, Q. Zhao, X. Tan, I.M. Reaney, Bismuth ferrite-based lead-free ceramics and multilayers with high recoverable energy density. J. Mater. Chem. A **6**, 4133–4144 (2018)
42. Z. Chen, X. Bai, H. Wang, J. Du, W. Bai, L. Li, F. Wen, P. Zheng, W. Wu, L. Zheng, Y. Zhang, Achieving high-energy storage performance in $0.67Bi_{1-x}Sm_xFeO_3$–$0.33BaTiO_3$ lead-free relaxor ferroelectric ceramics. Ceram. Int. (2020). https://doi.org/10.1016/j.ceramint.2020.01.181
43. L. Zhang, Y. Pu, M. Chen, T. Wei, W. Keipper, R. Shi, X. Guo, R. Li, X. Peng, High energy-storage density under low electric

fields and improved optical transparency in novel sodium bismuth titanate-based lead-free ceramics. J. Eur. Ceram. Soc. **40**, 71–77 (2020)
44. L. Zhang, Y. Pu, M. Chen, T. Wei, X. Peng, Novel $Na_{0.5}Bi_{0.5}TiO_3$ based, lead-free energy storage ceramics with high power and energy density and excellent high-temperature stability. Chem. Eng. **383**, 123154 (2020)
45. F. Li, R. Si, T. Li, C. Wang, J. Zhai, High energy storage performance and fast discharging speed in dense $0.7Bi_{0.5}K_{0.5}TiO_3$–$0.3SrTiO_3$ ceramics via a novel rolling technology. Ceram. Int. **46**, 6995–6998 (2020)
46. F. Li, T. Jiang, J. Zhai, B. Shen, H. Zeng, Exploring novel bismuth-based materials for energy storage applications. J. Mater. Chem. C **6**, 7976–7981 (2018)
47. Z. Yang, F. Gao, H. Du, L. Jin, L. Yan, Q. Hu, Y. Yu, S. Qu, X. Wei, Z. Xu, Y.-J. Wang, Grain size engineered lead-free ceramics with both large energy storage density and ultrahigh mechanical properties. Nano Energy **58**, 768–777 (2019)